Korean J. Chem. Eng., **30**(4), 771-786 (2013)
DOI: 10.1007/s11814-013-0033-8

INVITED REVIEW PAPER

Natural gas hydrate as a potential energy resource: From occurrence to production

Jiwoong Seol and Huen Lee†

Department of Chemical and Biomolecular Engineering (BK21 program) and Graduate School of EEWS, KAIST, 335, Gwahangno, Yuseong-gu, Daejeon 305-701, Korea
(*Received 19 January 2013 • accepted 26 February 2013*)

Abstract−Natural gas hydrate reservoirs have been strongly suggested as a potential energy resource. However, this potential is expected to be limited by geological factors, reservoir properties, and phase-equilibria considerations. Accordingly, sufficient understanding and accurate analyses for the complex surroundings in a natural gas hydrate system have to occur before methane recovery. In this paper, we discuss the formation and structure patterns of global natural gas hydrate, including the origins of hydrocarbon, crystal structures, and unique structure transition. We also summarize two important anomalies related to methane occupancy and chlorinity which were revealed very recently. Furthermore, we review the geological and chemical surroundings of the shallow hydrate deposits, the so-called brine patch discovered in the Cascadia Margin and Ulleung Basin, which are significantly related to tectonic conduits for methane gas and positive chlorinity.

Key words: Natural Gas Hydrate, Methane Occupancy, Chlorinity, Shallow Hydrate, Ulleung Basin

INTRODUCTION

It is generally assumed that oceanic gas hydrates contain a huge volume of natural gases. The most widely cited estimate of natural gases in global hydrates is 21×10^{15} m^3 of methane at STP (corresponding to about 10 Tt of methane carbon), which is proposed as a consensus value [1]. This large gas hydrate reservoir is further suggested as a potential (1) factor in global climate change, (2) submarine geo-hazard, and (3) energy resource [2]. Assessments of gas hydrate as an energy source have often been optimistic, based on worldwide occurrence in continental margins and the high methane content of natural gas hydrate. For energy recovery from natural gas hydrate, numerous studies have been done, such as thermodynamic analysis of methane hydrate [3,4] and recovery processes using unique swapping patterns induced by external CO_2 and CO_2/N_2 gas [5-7], and the results seem to be attractive. However, the important problem is that the real recovery processes are expected to be necessarily limited by geological factors, reservoir properties and phase-equilibria considerations. For the past decade, the regional gas hydrate stability zone (RGHSZ) has been found to have a very complicated geometry with significant variability due to lateral and vertical changes in pore water salinity and heat flow. Furthermore, the gas hydrate occurrence is noticed to be controlled by complex interaction of unique factors, such as temperature, pressure, salinity, and geochemical regime. Accordingly, sufficient understanding and accurate analyses for the complex surroundings in natural system have to occur before methane recovery.

Boswell and Collett suggested a gas hydrate resource pyramid that is commonly used to display the relative amount and productivity of different elements arranged with the most promising resources at the top and most challenging at the base [8]. Instead of Arctic sandstones at the top of the pyramid, oceanic gas hydrates generally can be classified into four types. The first one, deep-water sandstones, includes moderate-to-high concentrations of gas hydrates that may be challenged by the high costs of gas production due to the depth. The second one is the gas hydrate deposits generally found encaged in non-sandstones including fractured fine-grained muds and shales. The production of methane from this type of deposit has been considered to be technically problematic at the present stage. The third one is deep-seated hydrate disseminated in the RGHSZ, above the base of the gas hydrate stability zone (BGHSZ). Although this type of deposit hosts the largest fraction of total gas hydrate resources, this is at the very base of the resource pyramid because of poor permeability through fine-grained sediment and low saturations of gas hydrate (~10% or less) [9,10]. The concept of gas production from fine-grained sediments using gas-driving fracturing induced by thermal stimulation was suggested [10]. Santamarina and Jang reported that thermally dissociated gas with extensive volume can generate fractures and develop high permeability paths that can facilitate gas production in fine-grained sediments. However, most of the fine-grained gas hydrate systems are considered to have very poor reservoir potential [11]. The last and special one is locally-concentrated massive hydrate formed in shallow depth near the seafloor. Recently, it has been continuously discovered worldwide, but the accurate amount of this reservoir is unknown yet. It is particularly known to be associated with geological conduits which act as conduits for gases and fluids, for example, Horizon A at the southern summit of Hydrate Ridge, Cascadia Margin [12], and the seismic chimneys in the Ulleung Basin offshore Korea [13,14]. Shallow hydrate deposits associated with cold vents have been also reported in the Gulf of Mexico [15], the Nankai Trough [16], the Cascadia Margin [12,17,18], and the Ulleung Basin [19], where tectonic or diapiric faults provide fluid transport path. In several regions of near-seafloor hydrate, a unique signature of significantly enriched chlorinities (positive anomalies) was also detected.

†To whom correspondence should be addressed.
E-mail: hlee@kaist.ac.kr

In this paper, we discuss the formation and structure patterns of global natural gas hydrate including the origins of hydrocarbon, crystal structures, and unique structure transition. We also summarize two important anomalies related to methane occupancy and chlorinity, which were revealed very recently. Furthermore, we review the geological and chemical surroundings of the shallow hydrate deposits, the so-called brine patch discovered in the Cascadia Margin and Ulleung Basin, which are significantly related to tectonic conduits for methane gas and positive chlorinity.

FORMATION AND STRUCTURE TRANSITION PATTERNS OF NATURAL GAS HYDRATE

1. Biogenic and Thermogenic Hydrocarbon Sources

Hydrocarbon gases in natural gas hydrate are divided into two types according to their origin, biogenic and thermogenic hydrocarbons. The molecular composition (C_1/C_{2+}) of hydrocarbon gases in gas hydrate samples, coupled with measurements of carbon isotope of methane ($\delta^{13}C_{C1}$), provide a basis for interpreting the origin of this gas. They are defined as follows:

$$\frac{C_1}{C_{2+}} \equiv \frac{\text{mole fraction of } CH_4}{\text{mole fraction of } (C_2H_6 + C_3H_8 + \cdots)} \quad (1)$$

$$\delta^{13}C_{C1} \equiv \left\{ \frac{(^{13}C/^{12}C)_{sample}}{(^{13}C/^{12}C)_{PDB\ standard}} - 1 \right\} \times 10^3 (‰) \quad (2)$$

In most of the methane hydrate samples, methane has carbon-isotopic composition lighter than –60‰ ($\delta^{13}C_{C1}$<–60‰), suggesting that the methane is mainly of microbial origin. Isotopically lighter than –70‰ has not often been found in natural gas hydrate. Microbial methane in methane hydrate may have either been generated in place, have migrated only short distances, or been recycled during the concomitant process of hydrate formation and dissociation accompanying sediment [20]. This biogenic methane likely results from bacterial methanogenic processes, taking place in shallow sediment below the sulfate reduction zone, in which CO_2 is reduced to methane. The net reaction is represented by,

$$CO_2 + 8\,H^+ + 8e^- \rightarrow CH_4 + 2H_2O$$

The anaerobic reaction for consumption of methane and sulfate resulting in the production of carbonate in the sulfate reduction zone occurs as

$$CH_4 + SO_4^{2-} \rightarrow CO_3^{2-} + H_2S + H_2O$$

To much lesser extent, especially in oceanic sediment, acetate from organic matter is converted to methane by fermentation reactions.

$$CH_3COOH \rightarrow CH_4 + CO_2$$

The pathways of natural methane production are summarized in Fig. 1 and the range of expected carbon isotopic compositions of methane have been well discussed in detail by Whiticar et al. [21] and Whiticar [22]. The biogenic hydrocarbons generally have values of C_1/C_{2+} higher than 1000.

In contrast, methane with carbon isotopic compositions heavier than –60‰ ($\delta^{13}C_{C1}$>–60‰), accompanied by a significant amount of higher molecular weight hydrocarbons, such as ethane, propane and larger hydrocarbon gases, is thermogenic methane, according to

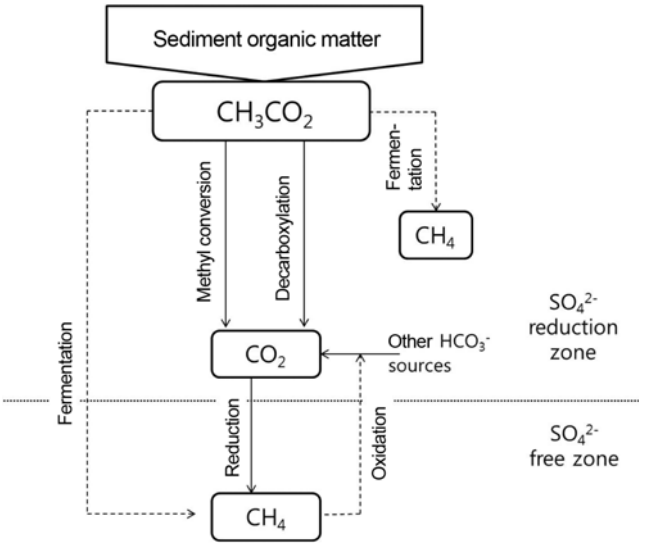

Fig. 1. Schematic of biogenic methane production in ocean sediment. Reproduced and modified with permission from [21, 22].

the criteria of Schoell [23]. This gas mixture results from the thermal decomposition of organic matter or petroleum at sediment depths greater than about 1,000 m at above 450 K. Thermogenic gases do not form hydrates at their site of production because the ambient temperatures are outside the hydrate stability. The thermogenic hydrocarbons have values of C_1/C_{2+} lower than 100. Thermogenic gas hydrates have been reported for the Gulf of Mexico [24], Caspian Sea [25], the southern summit of the Hydrate Ridge [26], the northern Cascadia Margin [27,28], and the East Sea [29]. At all these locations, hydrates formed with a high portion of allochthonous gas are massively accumulated near the seafloor. In contrast to the biogenic methane, the thermogenic hydrocarbons migrate long distances from deeply buried sediment to shallow sediment to form hydrates.

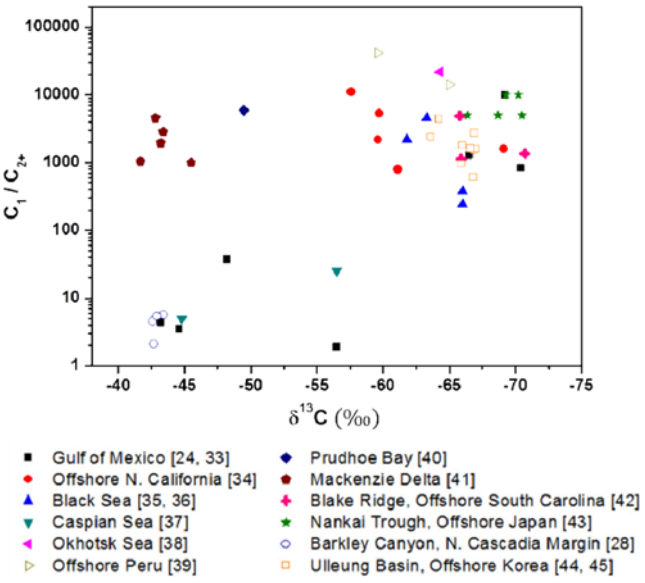

Fig. 2. The compositional and isotopical data of hydrocarbon gases from hydrate gas at various sites around the world.

Table 1. Stable carbon isotope and molecular composition of hydrate

Sample	C_1 (%)	C_2 (%)	C_3 (%)	i-C_4 (%)	n-C_4 (%)	i-C_5 (%)	n-C_5 (%)	$\delta^{13}C_{C1}$ (‰)	C_1/C_{2+}	Reference
Gulf of Mexico										
1	71.8	3.4	18.8	5.7	0.3	n.d.	n.d.	−44.6	2.5	Brooks et al. [24]
2	73.9	4.9	16.3	4.6	0.2	n.d.	n.d.	−44.8	2.8	
3	75.4	3.3	16.8	4.2	0.09	0.01	n.d.	n.a.	3.1	Davison et al. [46]
4	21.2	9.5	7.5	2.5	17.5	41.1	0.8	−29.3	0.27	Sassen and McDonald [31]
Northern Cascadia										
1	85.1	7.7	3.3	1.1	1.7	1.1		−43.4	5.7	Pohlman et al. [28]
2	81.9	10.4	3.7	1.2	2	0.8		−42.6	4.5	
3	84.3	9.1	3.2	1	2.2	2.2		−42.9	4.5	
4	68.1	10.8	12.5	4.2	2.2	2.2		−42.7	2.1	
5	75.4	11.4	5.7	1.2	2.2	0.7	0.3	−46	3.1	Lu et al. [48]

n.a., not available; n.d., not detected

Accordingly, thermogenic hydrates are generally concentrated near structural features in sediment, such as faults, vents and seeps, and diapirs, which serve as conduits for the migration of gas and fluid from deep sources such as petroleum reservoirs [30]. Oil-sustained yellow/orange color and thermogenic hydrates were discovered in the Gulf of Mexico [31,32] and northern Cascadia Margin [27,28]. Fig. 2 shows the data of compositional and isotopical analyses from various gas hydrate deposits worldwide.

2. sII and sH

Methane comprises more than 99% of the hydrocarbon gases in most natural gas hydrate. Minor quantities of CO_2 and H_2S are often present, but because the main gas component is methane, the natural gas hydrate is called methane hydrate which has sI crystallography. However, sII and sH hydrate have steadily been found in several regions, such as the Gulf of Mexico and Cascadia Margin.

Brooks et al. [24] analyzed the gas compositions of the samples recovered from the upper few meters of sediments in the northwestern Gulf of Mexico. Table 1 shows the results of isotopic and compositional measurement. The large amounts of propane and isobutene indicate the existence of sII hydrate. Davidson et al. [46] also estimated the gas component of the near-seafloor sample from the Gulf of Mexico and obtained similar results. Furthermore, they carried out ^1H and ^{13}C NMR and powder XRD measurement and confirmed the sII hydrate. The sII hydrate made up more than 80% of the water in the core materials (80.5 wt% water, 13.6 wt% gas and 5.9 wt% solid residue), and no sI hydrate was detected in their result. The thermodynamic nature of the hydrate collected from Gulf of Mexico is indicated by (1) gas compositions containing large amounts of heavy hydrocarbons (C_{2+}), (2) carbon isotopic compositions ($\delta^{13}C_{C1}$>−60‰), and (3) the presence of oil in the cores [24]. The large amounts of non-methane gases (C_{2+}) sufficiently stabilize the hydrate to exist even outside of the methane hydrate stability conditions. For example, a hydrate sample was recovered in the part of Gulf of Mexico at 6-8 °C and water depth 530 m.

After a new structure (sH) was identified in the lab experiments by Ripmeester et al. [47], Sassen and McDonald [31] presented the first compositional evidence for the natural occurrence of sH hydrate from Bush Hill in the Gulf of Mexico. The hydrocarbon gas mainly originated from the thermogenic source ($\delta^{13}C_{C1}$~−29.3‰). The composition of i-C_5 which can only occupy the large cage of sH was over 40% (Table 1). It strongly supports the existence of sH hydrate. Pohlman et al. [28] also suggested evidence for sH hydrate in the Barkley Canyon, northern Cascadia. The molecular composition of the Barkley Canyon hydrate was primarily methane (68.1 to 85.1%) with significant quantities of thermogenic C_{2+} hydrocarbons (Table 1 and Fig. 2). The abundance of ethane, propane and iso-butane was an evidence of sII hydrate, and small quantities of C_{5+} hydrocarbons (0.8 to 2.2%) suggested the existence of sH hydrate as a minor constituent.

More recently, Lu et al. [48] showed that the sample from Bark-

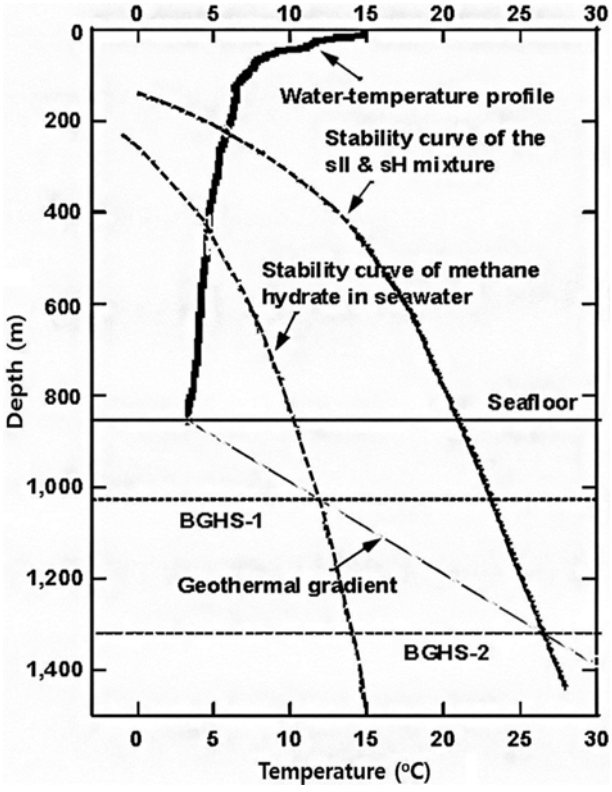

Fig. 3. The stability zones of methane hydrate and naturally occurring sII-sH complex gas hydrate from Barkley Canyon, offshore Vancouver Island. Reproduced with permission from [48].

ley Canyon on the northern Cascadia Margin contains sH hydrate and suggested direct evidence for the natural occurrence of sH hydrate with spectroscopic methods, such as powder XRD and solid-state ^{13}C NMR. The sH hydrate was intimately associated with sII hydrate, and the two structures contain more than 13 different hydrocarbon guests. Their research provided the first confirmation of the existence of natural sH hydrate with direct structure analyses, although Sassen and McDonald [31] and Pohlman et al. [28] suggested the compositional evidence. Table 1 shows the isotopic data ($\delta^{13}C_{C1}$~−46‰) and fractional abundance of methane (C_1/C_{2+}~3.1), which indicate the thermogenic origin of enclathrated hydrocarbons.

The sII and sH hydrates are much more stable than sI methane hydrate. Accordingly, the region where these hydrates could be found is greatly expanded over that of sI methane hydrate, passively appearing at a depth of about 500 mbsf in the Barkley Canyon region [48] (Fig. 3). Because the thermogenic hydrocarbons are generated at about 1,000-2,000 mbsf (or even deeper) and migrate upward in the sedimentary column, the thermogenic hydrates are expected to exist as deep as their stability would allow, even below the GHSZ of sI methane hydrate [24,48].

3. Structure Transition of NGH by External Methane Attack

As discussed before, sII and sH hydrates with heavy hydrocarbons (C_{2+}) show much more stable equilibrium PT conditions than sI hydrate, which was also experimentally revealed on a laboratory scale [49]. The inclusion of large hydrocarbons induces a hydrate formation condition to be more favorable by lowering the pressure and raising the temperature to form the mixed hydrate compared with the corresponding condition of pure methane hydrate (Fig. 4). However, Yeon et al. also suggest the opportunity for the structural transition of sII and sH hydrates into sI methane hydrate driven by an external methane attack. They first prepared the sII hydrate with CH_4+C_2H_6 and sH hydrate with CH_4+(methylcyclohexane or isopentane) and next, pressurized them with pure methane gas at about 273 K. Then, the previously constructed sII and sH frameworks were significantly transformed into sI methane hydrate within three days, as supported by spectroscopic analyses (XRD, NMR, and Raman spectroscopy). The results are shown in Fig. 4. Distinctively, the larger methane attack (higher pressure of external methane) made a much more structural transition into sI hydrate. As mentioned before, even if the sII and sH hydrates containing heavy hydrocarbon (C_{2+}) are more abundant than those that have been discovered at the present level [24,48], most of sII and sH will ultimately be transformed into sI methane hydrate under free methane-rich surroundings (by such as *in-situ* biogenic methane) sealed by an overlying impermeable hydrate layer. Yeon et al. [49] suggested that their results could be a reason for the preponderance of sI among the complex structures of natural gas hydrate. In these respects, more precise and considerable approaches will be needed to investigate the complicated struc-

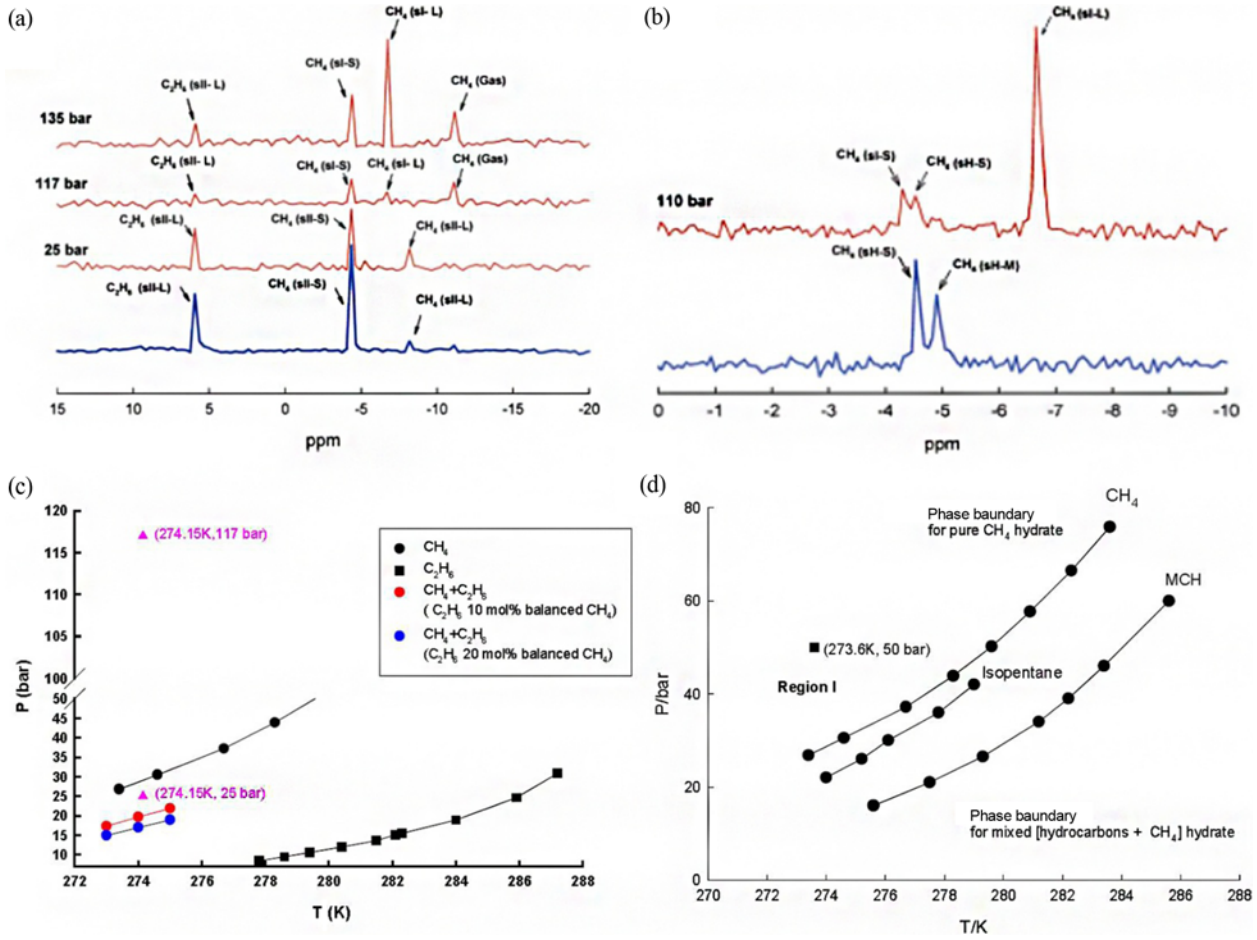

Fig. 4. (a) and (b), solid-state NMR data of sII and sH hydrate attacked by external methane gas; (c) and (d), equilibrium P-T conditions of sI, sII, and sH hydrate. Reproduced and modified with permission from [54].

ture of natural gas hydrate.

CIRCUMSTANCES OF NATURAL GAS HYDRATE LAYER

1. Abnormal Methane Occupancy Induced by Intercalated Sediment Structure

As mentioned above, the complex origins and structures of natural gas hydrate under the ocean floor have been extensively studied for several decades. However, thermodynamic phase behavior and structural characteristics must still be considered to understand the physicochemical and mineralogical aspects of the natural gas hydrate in marine sediments that necessarily coexisted with sediments. According to Santamarina and Jang [10], most submicron-size grains are made of clay minerals formed through chemical processes, for example, fine-grained layers in Gulf of Mexico and Blake Ridge. Non-clay minerals larger than 50 μm are formed through mechanical processes, for example, coarse-grained layers in Mackenzie Delta and Nankai Trough. Biological activity may contribute shell fragments and microfossils to the sediments, leading to a dual porosity medium, for example, Blake Ridge and East Sea [10].

Among various clay minerals, the smectite group, known as montmorillonite, belongs to a 2 : 1 phyillosilicate composed of two tetrahedral sheets separated by one octahedral sheet [50,51]. In smectite clays, there are two representative types, Wyoming- and Cheto-type montmorillonites, which differ primarily in the population of their octahedral layers, particularly regarding the amount of octahedral Mg [50,52]. Many molecular dynamic simulation studies of clathrate hydrates have focused on investigating the role of clay minerals in methane hydrate formation, while it has yet to be confirmed whether clay sediments play a specific role in shifting the hydrate formation conditions of intercalated methane hydrate (IMH) to a more favorable direction. Most of the modeling results suggested that clay sediments promote hydrate formation. On the contrary, reported experimental data can be divided into three patterns: promotion [51, 53-55], inhibition [56,57], and no effect [58,59].

Among these studies, Yeon et al. [54] and Seo et al. [55] suggested that the IMHs are significantly affected by interlayer cations of clay, such as Na^+ and Ca^{2+}. For the first, Seo et al. suggested that the equilibrium PT conditions of IMHs in Cheto-type clays were not considerable but sufficiently promoted compared to those of pure methane hydrate (Fig. 5(a)). Moreover, Seo et al. observed, at a clay mass fraction above 25 wt%, that the promotional trend disappeared, implying that a certain value of upper limit exists in the clay concentration of promotion effect.

Next, more importantly, Yeon et al. [54] discovered the unique features of methane hydrate intercalated in Wyoming- and Cheto-type clays. They suggested that, because clay minerals have a layered structure with unit layers that are approximately 1 nm thick (~1.2 nm) and contain interlayer cations inside, the properties of methane hydrates confined in the clay interlayer are largely different from those of methane hydrate in bulk. The clay interlayer d-spacing swelled to 1.6 nm when the sI methane hydrate (lattice parameter a=11.897± 0.002 Å) was formed inside the layer, as confirmed with cryo-TEM image and powder XRD. To identify the actual nature of IMH, they estimated the solid-state ^{13}C NMR spectra of methane hydrate in

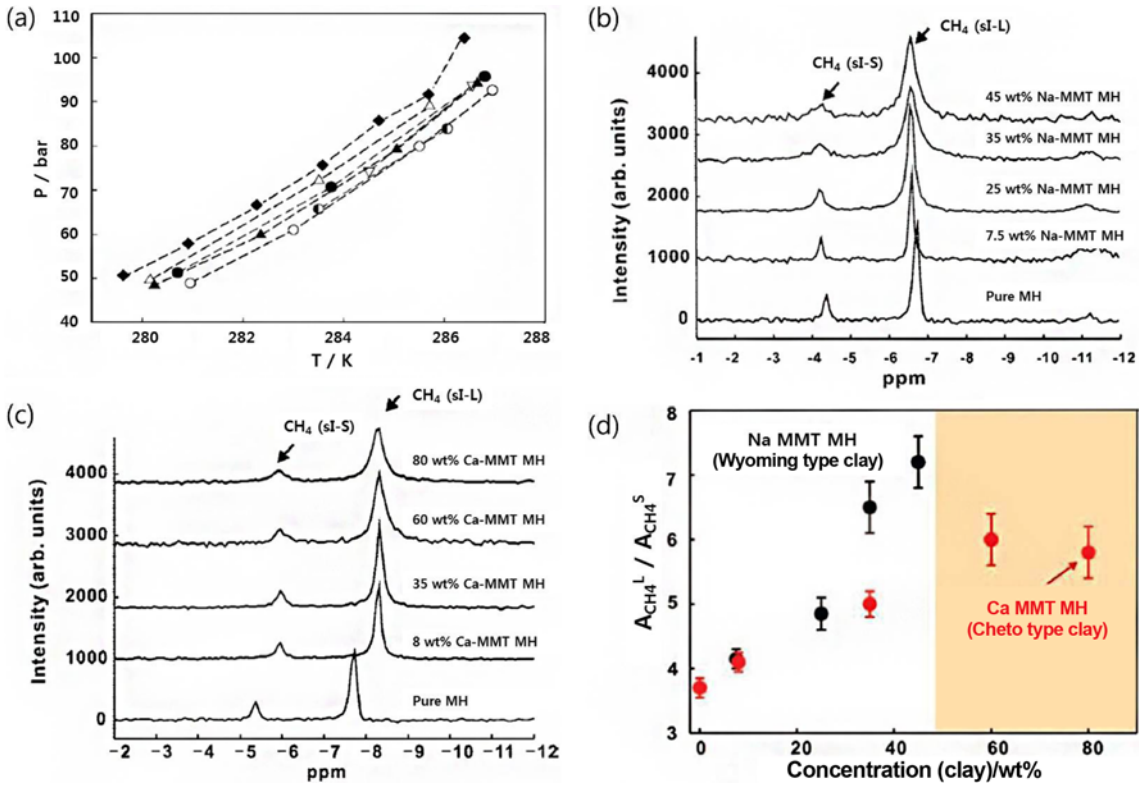

Fig. 5. (a), Phase equilibrium condition of methane hydrate with various clay contents; (b) and (c), ^{13}C NMR data of IMH with various contents of Na- and Ca- montmorillonite; (d), Area ratios of large to small cage obtained from (b) and (c). Reproduced with permission from [54,55].

Wyoming- and Cheto-type clays (Na- and Ca- montmorillonite, respectively). Basically, the chemical shifts of ^{13}C NMR were revealed to about −6.7 ppm and −4.3 ppm for CH_4 in sI-L and sI-S cages, respectively. As shown in Figs. 5(b) and (c), the methane occupancy ratio of large to small cages in sI methane hydrate was significantly changed according to the clay concentration. The ^{13}C NMR peak area ratio of large to small cages of bulk sI methane hydrate is known to be about 3.7. However, the corresponding ratio in Na-montmorillonite increases with the clay concentration, up to 7.1 for 45 wt% Na-montmorillonite. In the other case, the ratio was increased up to 6 for 60 wt% Ca-montmorillonite. The overall results are summarized in Fig. 5(d). This result surprisingly suggested that significant portions (up to about 60%) of small cage in IMH were not occupied by a methane guest. In other results of the ^{27}Al, ^{29}Si, and ^{23}Na MAS NMR spectra from Yeon et al. [54], the ^{23}Na peak of interlayer Na^+ cation in swollen Na-montmorillonite was far different from that in the dry one, while the ^{27}Al and ^{29}Si peaks in the layered crystal structure of clay showed no change. Accordingly, Yeon et al. concluded that the interlayer cations of clay sediment, such as Na^+ and Ca^{2+}, may considerably affect the abnormal cage occupancy of IMH, and moreover, similar results were detected in the real samples drilled from the East Sea, offshore Korea (see below Chapter 4.2).

2. Abnormal Chlorinity Observed in Several Sites

Hydrates, like normal ice, exclude the sea salts from their crystal structure. When methane and water form hydrates in the sediment pore space, the salinity (more specifically the chlorinity) of the pore water increases because of the withdrawal in the hydrates of water (but not salts) from the pore water pool. However, more complicated chlorinity patterns have been detected in natural circumstances over the past few decades. Negative or positive anomalies of chlorinity are usually discovered in deep sea sediments related to methane hydrate with complex effects of burial compaction, diffusion, advection and so on.

Ussler and Paull [60] suggested that the concentration of a nonreactive species such as Cl^- anion after gas hydrate decomposition can be computed by using the following equation:

$$C_d = C_{pw}\left(1-\frac{V_h}{(w-(w-1)V_h)}\right)+C_h\left(\frac{V_h}{(w-(w-1)V_h)}\right) \quad (3)$$

where C_d is the concentration after decomposition, C_{pw} is the pore water concentration prior to decomposition and V_h is the volume fraction of hydrate filling the pore space. C_h means the concentration in the gas hydrate, which can be simply assumed to be zero. If gas hydrate is formed in a geometrically closed system, the concentration of the Cl^- anion can be simply calculated as follows:

$$C = \frac{C_i}{1-\left[\frac{V_h}{(w-(w-1)V_h)}\right]} \quad (4)$$

where C_i is the initial ion concentration of the pore fluid and C is the ion concentration after filling a volume fraction of the pore volume, V_h, with gas hydrate. In the equations above, w is defined to represent the occupancy-density characteristics of the formed gas hydrate with the value of 1.264 assuming full occupancy. In natural circumstances, C_{pw} will not be the same as because diffusive or advective loss or gain within the dissolved ion pool occurs after gas hydrate formation. Eq. (3) can be applied to estimating the amount of gas hydrate formed in sediment pore space if the C_{pw} can be measured with reasonable certainty. Fig. 6 shows the relationships between the salt (chloride concentration) and the volume fraction of gas hydrate. Ussler and Paull [60] also calculated the amount of gas hydrate using these equations and various chloride concentration data from DSDP/IODP sites.

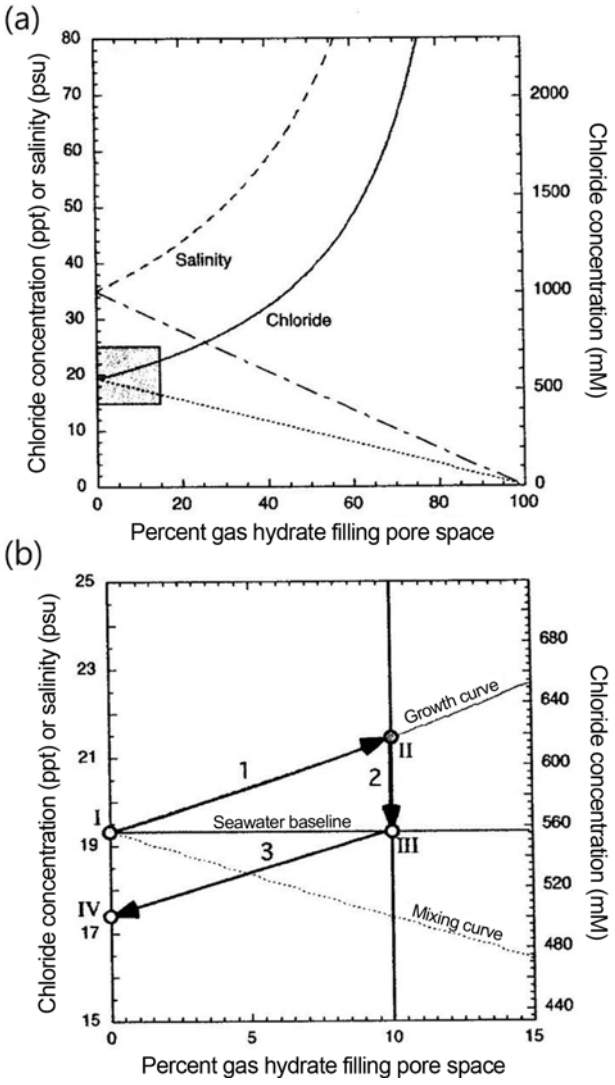

Fig. 6. Scheme of salinity (chlorinity) freshening by hydrate dissociation during sampling from drilling cores. Reproduced with permission from [60].

In this respect, since the first time that the chloride concentration data for pore water believed to be associated with gas hydrate were obtained from DSDP Legs 66 and 67 [61,62], low chloride anomalies have been used to identify the former presence of gas hydrate and to estimate the amount of gas hydrate for decades. Decreasing trends with depth in hydrate-bearing sediment have been observed in Blake Ridge DSDP Leg 76 [63,64], ODP Leg 164 [65], offshore from Guatemala DSDP Leg84 [66,67], offshore from Peru ODP Leg 122 [39], the Cascadia Margin ODP Leg 146 [68], and the Mackenzie Delta Mallik 2L-38 well [69]. These chlorinity trends are derived by a large amount of fresh water from the dissociation

of gas hydrate during core recovery. Accordingly, pore water freshening is a useful signal for the presence of gas hydrate although other processes can cause pore waters to decrease chlorinity. However, recently, pore waters with significantly enriched chlorinity coexisting with the massive near seafloor hydrate were discovered in several sites, representatively, in the Hydrate Ridge offshore Oregon, and Ulleung Basin offshore Korea (for detailed phenomena, see below Chapters 4.1 and 4.2).

Over the past few years, several researchers have suggested numerical models to simulate gas hydrate formation in marine sediments associated with salt exclusion [70,71]; however, they focused on the negative chloride anomaly. Haeckel et al. presented an extraordinarily enriched chlorinity (up to 809 mM in pore water versus 543 mM in seawater) from the sample drilled on the near seafloor at the southern summit of the Hydrate Ridge [72]. They quickly separated the solid hydrate from the surrounding sediment-pore water system and minimized the release of fresh water from hydrate dissociation to preserve the excluded chloride. They also suggested a numerical transport-reaction model to simulate the positive chloride anomalies and calculated the hydrate formation rate (0.15-1.08 $mol \cdot cm^{-2} \cdot yr^{-1}$, corresponding to 1.5×10^{3}-1.08×10^{4} $mol \cdot m^{-2} \cdot yr^{-1}$). It is orders of magnitude larger than previously reported values (~10^{-3} $mol \cdot m^{-2} \cdot yr^{-1}$) for deep seated hydrate [70,71]. The estimated rate can build up a hydrate layer with a thickness of 30-40 cm within 4-10 weeks. This formation rate cannot be achieved by the diffusion of dissolved methane alone; thus, near-seafloor methane hydrate should be precipitated from methane gas bubbles: 0.2-1.3 gas bubbles per cm^3 of bulk sediment permanently present, as calculated by the aforementioned researchers. Torres et al. [73] also developed a one-dimensional, non-steady state, transport-reaction model to simulate the observed chloride enrichment at Site 1249 (see Chaper 4.1 for details). Similar with the result from Haeckel et al. [72], they show that methane must be transported in the gas phase from the depth of the BSR to the seafloor in order to reach the observed high chlorinity (up to 1,368 mM). The kinetic constants of methane hydrate formation were dependent on depth below the seafloor and the formation rate was higher in shallow depth because the force of hydrate crystallization can overcome effective overburden stress.

According to the results of simulation, most of the methane hydrate observed with highly chloride enriched pore water is likely to form from methane free gas rather than dissolved methane. Although the formation of gas hydrate from dissolved gas in natural porous media was revealed experimentally by Buffett and Zatsepina [74], dissolved methane seems to be not enough for reported positive Cl^- anomalies. For a different point of view, several studies revealed that highly enriched chlorinity could make methane free gas transport through the regional gas hydrate stability zone (RGHSZ) to the seafloor.

Liu and Flemings [75] proposed a thermodynamic equilibrium model to explain that free gas migration can be available due to the highly enriched chloride. The L+H solubility increases downward from the seafloor, while the L+G solubility slightly increases upward to the seafloor. At the intersection of the two curves, three phases exist in equilibrium and the solubility of methane reaches a maximum. This is the base of the GHSZ with chlorinity of 550 mM (Fig. 7(a)). When the concentration of dissolved methane exceeds the solubility, methane hydrate is stable over the BGHSZ while free gas is stable beneath the BGHSZ. If the chlorinity increases from

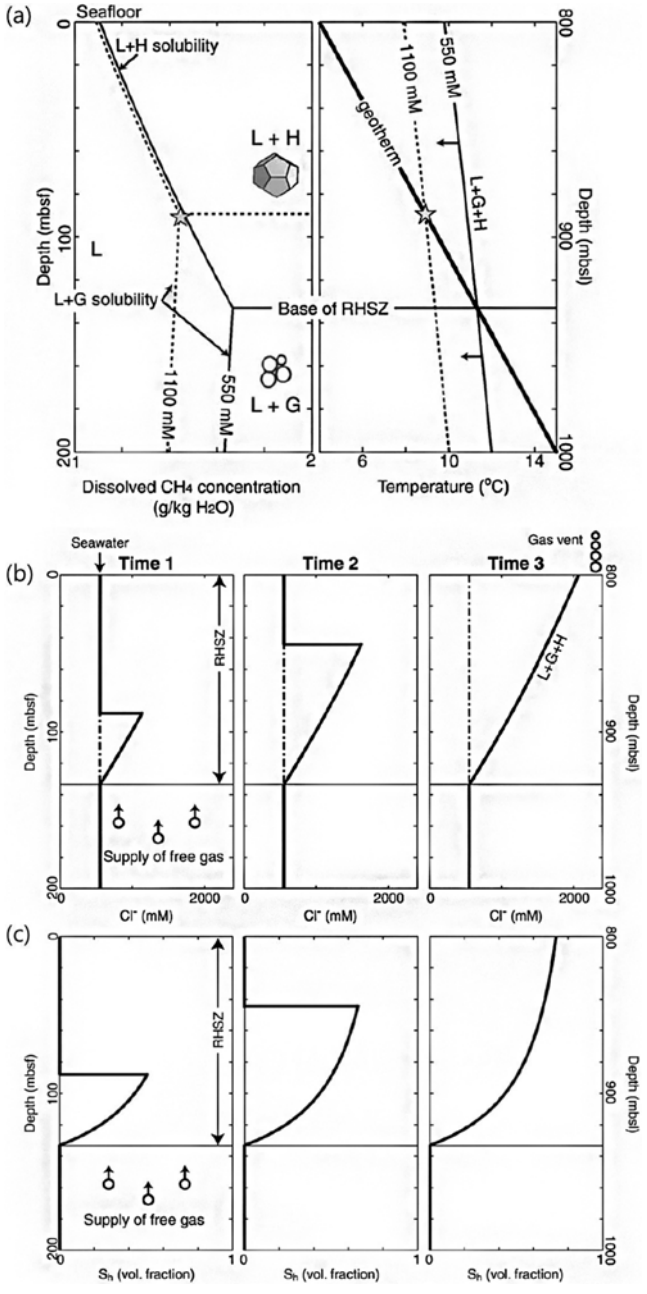

Fig. 7. Schematic of relationships between chlorinity and volume fraction of hydrate in pore space (S_h) with thermodynamic equilibrium modeling. Reproduced with permission from [75].

550 to 1,100 mM, the solubility of L+G reduces by ~15%, although that of L+H does not change notably. Accordingly, the BGHSZ shifts upward from 130 to 90 mbsf (Fig. 7(a)). Highly enriched pore water chlorinity makes the hydrate unstable, as anticipated.

Figs. 7(b) and (c) describe the evolution of hydrate saturation and chlorinity with time when the free gas is supplied below the BGHSZ. Just above the BGHSZ because the P-T conditions are close to the three phase boundary for sea water salinity (~550 mM), only a small amount of hydrate forms before chlorinity is enriched to the three phase boundary. The chlorinity needed to achieve a three-phase equilibrium increases upward toward the seafloor and has a

maximum value just below the seafloor; accordingly, more hydrate can be formed toward the seafloor. The chlorinity required for three-phase equilibrium is not achieved until hydrate saturation increases to ~70% near the seafloor. Once the three-phase boundary reaches the seafloor, it could be assumed to be a steady state (time 3). At that time, no more hydrate accumulates because the amount of methane supplied from below the BGHSZ becomes equal to that released at the seafloor. Eventually, a continuous methane migration channel, the so-called gas chimney, is constructed from near the BGHSZ to near the seafloor. Liu and Fleming [75] noted that this is an equilibrium model; thus, the gas hydrate saturation and chlorinity profiles are only determined by the inherent pressure and temperature profiles of RGHSZ. In contrast, the gas supply rate determines how fast the three-phase boundary propagates through the RGHSZ with respect to kinetics.

From another viewpoint, fractures, through which the free gas migrates, nucleate when the excess pore pressure exceeds the vertical hydrostatic effective stress as hydrate saturation increases [76]. Daigle and Dugan simulated salinity-sustained multiphase fluid flow at Hydrate Ridge (gas-dominated system) and Blake Ridge (water-dominated system). At Hydrate Ridge, free gas enters the RGHSZ and migrates upward by fracturing the sediment as hydrate forms and salinity increases and eventually vents to the seafloor. However, at Blake Ridge, free gas cannot enter the RGHSZ because water flux removes excess salt before it reaches three phase equilibrium. Free gas can initiate fractures only at the BGHSZ and it makes the highest S_h (hydrate volume fraction in pore space) at the BGHSZ and relatively very low S_h throughout the RGHSZ.

In summary, the supply of free gas enriches chlorinity in pore water induced by massive methane hydrate formation, and enriched chlorinity makes free gas migrate constituently through the RGHSZ. To accurately establish the chlorinity intimately related to the existence of free gas and the amount of methane hydrate (S_h), an *in-situ* chlorinity measurement is required to avoid hydrate dissociation during sampling [77]. Recently, Seol et al. [78] designed a chlorinity measurement system under *in-situ* conditions of the deep sea floor pressure and temperature. They measured the chlorinity during methane hydrate formation and controlled the formation rate with the contact area between methane gas and sediment. The chlorinity increased under a fast formation rate; however, no noticeable change was detected under a relatively low rate. The result showed that the methane hydrate formation rate should be maintained at least ~10^2 mol•cm^{-2}•yr^{-1} to enrich chloride and maintain the elevated chlorinity in pore fluid. Although their experimental system did not perfectly reflect all the external variables including hydrological, geometrical and physical circumstances of a deep-sea environment, they provided insight into the development of abnormal positive chlorinity in natural system as the first experimental attempt.

CASE STUDY

1. Southern Summit of the Hydrate Ridge Offshore Oregon, ODP Leg 204

The Hydrate Ridge is an accretionary ridge of the Cascadia subduction zone off of the Oregon coast, where the oceanic Juan de Fuca plate is subducted beneath the continental North American plate. Hydrate Ridge has been the target of the Ocean Drilling Program, Leg 146 and more recently Leg 204, thus underlying the importance of this area for gas hydrate research. Hydrate deposits and numerous vents where gas bubbles and fluids are released into the seawater have been discovered at Hydrate Ridge [17,79].

Milkov et al. reported molecular and isotopic properties of hydrate-bound gases from 55 samples and void gases from 494 samples collected during Ocean Drilling Program (ODP) Leg 204 [26]. In an area of high gas flux at the southern summit of the ridge (Site 1248-1250), shallow (0-40 mbsf) gas hydrates are composed of mainly allochthonous mixed microbial and thermogenic methane (>99%) and a small portion of thermogenic C_{2+} gases (up to about 0.4%), that migrated vertically and laterally from as deep as 2 to 2.5 km depths. Tréhu et al. [80] suggested that the seismic Horizon A has a role as a migration conduit that supplies fluids into the GHSZ and a feed seepage at the southern summit of Hydrate Ridge. This horizon was drilled on Leg 204 and was found to represent a relatively permeable layer of sand and ash with significant gas saturation [12]. In contrast, deep (50-105 mbsf) gas hydrates at the southern summit (Site 1248 and 1250) and on the flanks of the ridge (Site 1244-1247) are formed mainly from *in-situ* generated microbial methane and ethane [26].

Kim et al. [81] revealed the structure of natural gas hydrate sample collected at Site 1249 on ODP Leg 204 with XRD, solid-state ^{13}C NMR, and Raman spectroscopy. The results indicate that the examined sample was sI methane hydrate and cage occupancies were found to be about 99% for large cages and 80% for small cages. Hester et al. [82] measured the near seafloor hydrates at Hydrate Ridge using a seagoing Raman spectrometer for the first time. The natural hydrates measured were sI structure with methane as the predominant guest and cage occupancy ratios varied from 1.01 to 1.30. It is possible for a small amount of sII hydrate to exist due to existence of propane in some of the gas hydrate samples [26]. However, sII hydrate was not found in the laboratory analysis and the seagoing Raman spectrometer [81,82].

At ODP Sites 1244, 1245, 1247, 1248 and 1251, the chlorinity profiles showed no or negative anomalies relative to seawater level, with low methane hydrate contents. However, at the summit of Hydrate Ridge (ODP Sites 1249 and 1250), especially ODP Site 1249, pore fluids were highly enriched with chloride from near the sediment surface (~1 mbsf) to a depth of 25±5 mbsf, including massive methane hydrate deposits. Below this depth, chlorinity approaches sea water level including somewhat negative anomalies [12,18,83] (Fig. 8(a)). The value of enriched chlorinity measured from dry-looking samples using traditional shipboard methods was 1,370 mM [12]; however, this should be considered as minimum. Milkov et al. [18] suggested that the *in-situ* chlorinity was at least 1650 mM based on data from the pressure core sampler (PCS), Core 204-1249F-4P. Liu and Flemings [75] also calculated that the chlorinity between the seafloor and 50 mbsf is up to 2,600 mM.

As mentioned in Chapter 3.3, several researchers concluded with their models and experiments that methane transport in gas phase is needed to form massive hydrate and enrich the chloride [72,78, 83]. The results match well with the natural surroundings of Hydrate Ridge. High gas hydrate content (30-40% of pore volume or 20-26% of total volume) was detected near the seafloor (up to ~25 m) at the summit (Sites 1249 and 1250), while the average gas hydrate content below this depth was 2-5% of the pore volume [83]. PCS

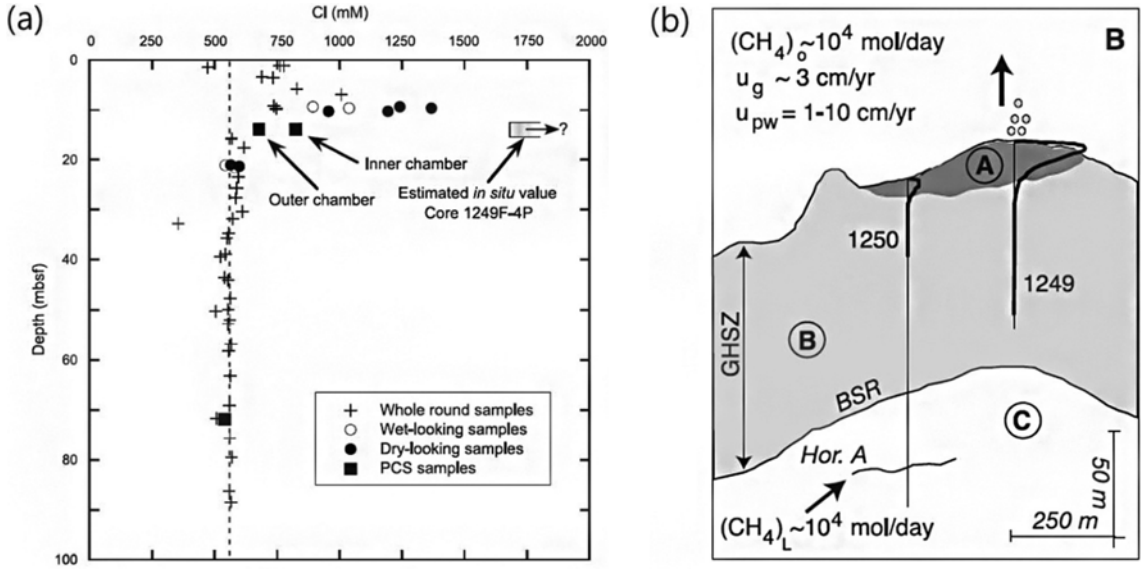

Fig. 8. (a), Chloride data from ODP Leg Site 1249; (b), Schematic of mass transfer occurring in the southern summit of Hydrate Ridge. Reproduced with permission from [18,73].

data from Site 1249 provides unique evidence of the natural coexistence of gas hydrate, hypersaline pore water, and free gas [18]. Considering all information gathered from PCS data, sediment pore space consisted of 40% gas hydrate, 50% hypersaline pore water ($[Cl^-]$>1,800 mM), and 10% free gas. Hester et al. [82] also revealed the existence of varying quantities of free methane gas with their seagoing Raman analysis.

Actually, a methane vent at the southern summit of Hydrate Ridge was discovered, and the amount of methane discharge from the seafloor was estimated to be ~10^4 mol•day^{-1} [84]. Tréhu et al. [83] estimated the amount of methane trapped in the hydrate deposits between the seafloor and 30 mbsf to be 1.5-2×10^8 m^3 (corresponding to ~ 10^{10} mol) at STP. Assuming hydrate saturation and steady state, the methane supply rate is sufficient to form the total amount of hydrate deposits currently present at the summit of Hydrate Ridge within a time scale of 500 years (Fig. 8(b)). Moreover, the hydrate formation rate near the seafloor is in the order of 10^2 mol•m^{-2}•yr^{-1}. Torres et al. [82] suggested that the massive hydrate observed within shallow depth is driven primarily by a decrease of overburden stress in near surface sediments. The gas bubble and hydrate pressure will exceed the overburden effective stress and push away sediment particles to form larger hydrate crystal. Torres et al. also proposed that shallow massive hydrate deposits on Hydrate Ridge or elsewhere require methane transport in gas phase at least to the depth where bubble and hydrate pressure exceeds the effective overburden stress.

Integrating most available geological, geophysical, and geochemical data, Milkov et al. [85] developed a reasonable model of gas hydrate formation at the southern summit of Hydrate Ridge, as shown

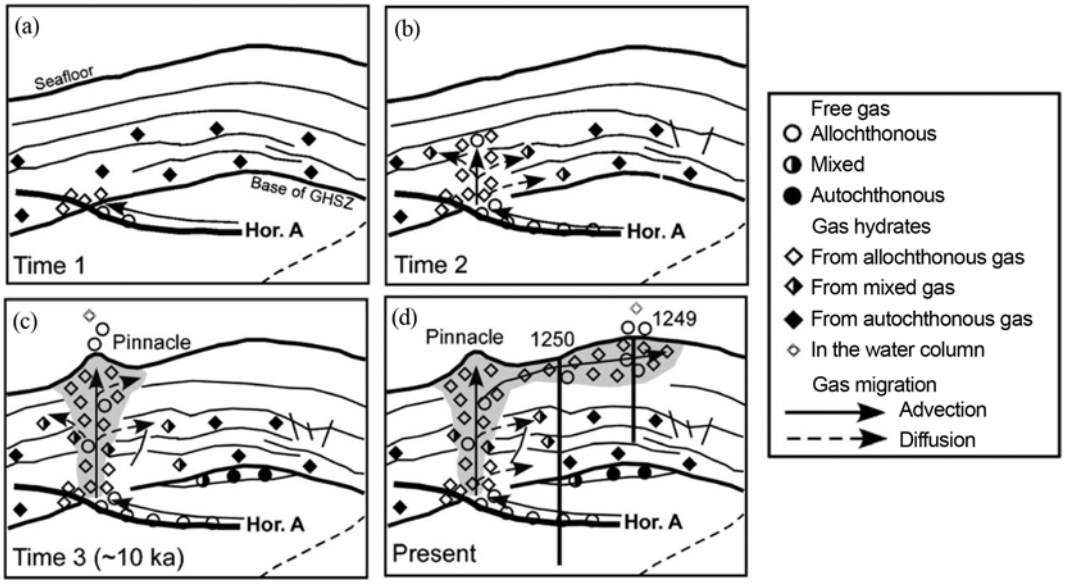

Fig. 9. Scenario of the evolution of a brine patch observed at Hydrate Ridge. Reproduced with permission from [85].

in Fig. 9. When free gas migrated though the permeable Horizon A and reached the intersection of Horizon A and BGHSZ, gas hydrate started to precipitate (Fig. 9(a)). As free gas was vertically supplied into the RGHSZ, the hydrate propagated and eventually reached the seafloor (Fig. 9(b)). The authigenic carbonate pinnacle [86] formed at the seafloor, which has very low permeability and acted as a seal for gas migration (Fig. 9(c)) [87]. This was evidenced by the lack of gas bubbles coming from the pinnacle area [86,88]. The gas laterally migrated to the crest of the anticline driven by buoyancy and precipitated gas hydrate (Fig. 9(d)). Pore water became highly enriched due to extensive hydrate formation, and no more hydrate could precipitate at the given temperature and pressure because of the enriched chlorinity [18,75,76]. The free gas erupted to the seawater from the seafloor of Site 1249 [88]. However, the fundamental questions related to complicate mechanisms for gas transport and chlorinity enrichment remain unanswered.

2. Ulleung Basin of the East Sea Offshore Korea

The Ulleung Basin is a deep, bowl-shaped, back-arc basin bounded by the steep continental slope of the eastern Korean Peninsula to the west and the southern Korea Plateau to the north. Extensive geophysical surveys have been conducted to find gas hydrate deposits in the Ulleung Basin since the late 1990s. The existence of gas hydrate was indicated by the presence of bottom simulating reflectors (BSRs) on multi-channel seismic profiles [89]. Generally, BSRs occur at the interface between overlaying hydrate-bearing sediments with high velocity and underlying gas-bearing sediments with lower velocity. This reflection coincides with the depth predicted from the phase diagram as the BGHSZ. Thus the BSRs are the most commonly used geophysical indicators of marine gas hydrates and are often used to provide an initial indication of potential gas hydrate distribution. More recently, gas hydrate has been confirmed by piston coring, drilling expeditions [13,19,44,45,90,91] and laboratory spectroscopic analysis [92].

During Ulleung Basin Gas Hydrate Expedition 1 (UBGH1), hydrate-bearing sediments were recovered from three sites (UBGH1-4, UBGH1-9, and UBGH1-10). At one site, a 130-meter thick hydrate-bearing sediment of interbedded sands and clays was penetrated, which is one of the thickest hydrate-bearing intervals to be documented worldwide [93]. Varying gas hydrate saturation with depth and a wide variety of lithologies were revealed from the drilled core at UBGH1-9 [90]. Negative chloride anomalies compared to the *in-situ* background chloride level were also observed between 63-151 mbsf. Hydrate saturations were estimated from the chlorinity anomalies up to 63.5% of pore volume with an average of 9.9%. Bahk et al. [19] concluded that the gas hydrate occurs in two different types in this zone. In Facies Association I (FA I) (0-98 mbsf) consisting mainly of alternating thin to medium bedded hemipelagic mud and turbidite sand or mud beds, the pore-filling type is preferentially associated with turbidite sand beds filling the pore space. The fracture-filling type formed as vein or nodule types occurs with filling fractures and faults of FA III (126-178 mbsf) composed of mostly diatomaceous hemipelagic mud without discrete turbidite sand layers. However, abnormally low gas hydrate saturations were detected in the interval FA II (98-126 mbsf) despite the dominance of turbidite sand or sandy debris flow bed which could have enhanced hydrate formation with low capillary force.

Compositional and structural analyses of gas hydrate samples revealed that they consist of sI hydrates containing more than 99% of biogenic methane. As discussed in Chapter 2.1 and shown in Fig. 2, the estimated $\delta^{13}C$ values of methane are between −60 and −80‰ and C_1/C_{2+} ratios are over or around 1000, which suggests that hydrocarbons discovered in the Ulleung Basin are preferentially generated by microbial reduction of CO_2 [19,44,45]. Bahk et al. [19] confirmed all the crystal structure of hydrate samples collected from five piston cores (P06, P08, P11, P12, and P18 from UBGH1) to be Pm3n structure I using powder XRD measurement. Based on the NMR and FT-Raman spectroscopic analysis, they suggested that the cage occupancies were about 0.99 for large cages and 0.65-0.85 for small cages (Table 2).

Yeon et al. [92] evaluated the cage occupancy ratio of three gas hydrate samples from P06, P08, and P12 with solid-state ^{13}C NMR (Fig. 10 and Table 2). They focused on the hydrate in the sediment-rich part of the natural sample based on their previous result from artificial intercalated methane hydrate (IMH) with clay minerals [54]. The two peaks of methane in sI-S (−4.3 ppm) and sI-L (−6.7 ppm) were the same for all the hydrates in both the white-looking hydrate-rich part and grey-looking sediment-rich part. For the hydrate-rich part, the area ratio of large to small cages ranged from 3.5 to 3.9 (corresponding to a cage occupancy ratio, θ_L/θ_S of 1.17 to 1.3), which is quite close to the ideal ratio of 3.75. In contrast, for the sediment rich part, the A_L/A_S ratio ranged from 5.4 to 7.1 (corresponding to θ_L/θ_S of 1.8 to 2.37), similar with that of the artificial IMH in their previous study. Yeon et al. [92] also compared the ^{23}Na chemical shift of sediment-rich hydrate with that of dried sediment. Peaks appeared at about −50 ppm for dry sediment and −25 ppm for hydrate-bearing sediment, and all the samples from P06, P08 and P12 showed the same pattern (Fig. 10(d)). Simultaneously, there was no change of chemical shift in ^{27}Al and ^{29}Si, which are covalently linked to oxygen and hydrogen atoms for the layered clay structure, between dried sediment and hydrate-bearing sediment. Yeon

Table 2. The structures and cage occupancy ratios of methane hydrate recovered from Ulleung Basin, UBGH1

GH-bearing cores	Structure	Cage occupancy ratios (θ_L/θ_S)			Description[a]	Notes[a]
		Overall[a]	GH-rich part[b]	Sediment-rich part[b]		
P06C	sI	1.53	1.3	1.8	Blocky nodules, massive layer and platy vein	Associated with acoustic blanking
P08C	sI	1.5	1.3	2.37	Blocky nodules and massive layer	Associated with acoustic blanking
P12C	sI	1.17	1.17	2.27	Platy veins	Associated with acoustic blanking

[a]Bahk et al. [19]
[b]Yeon et al. [92]

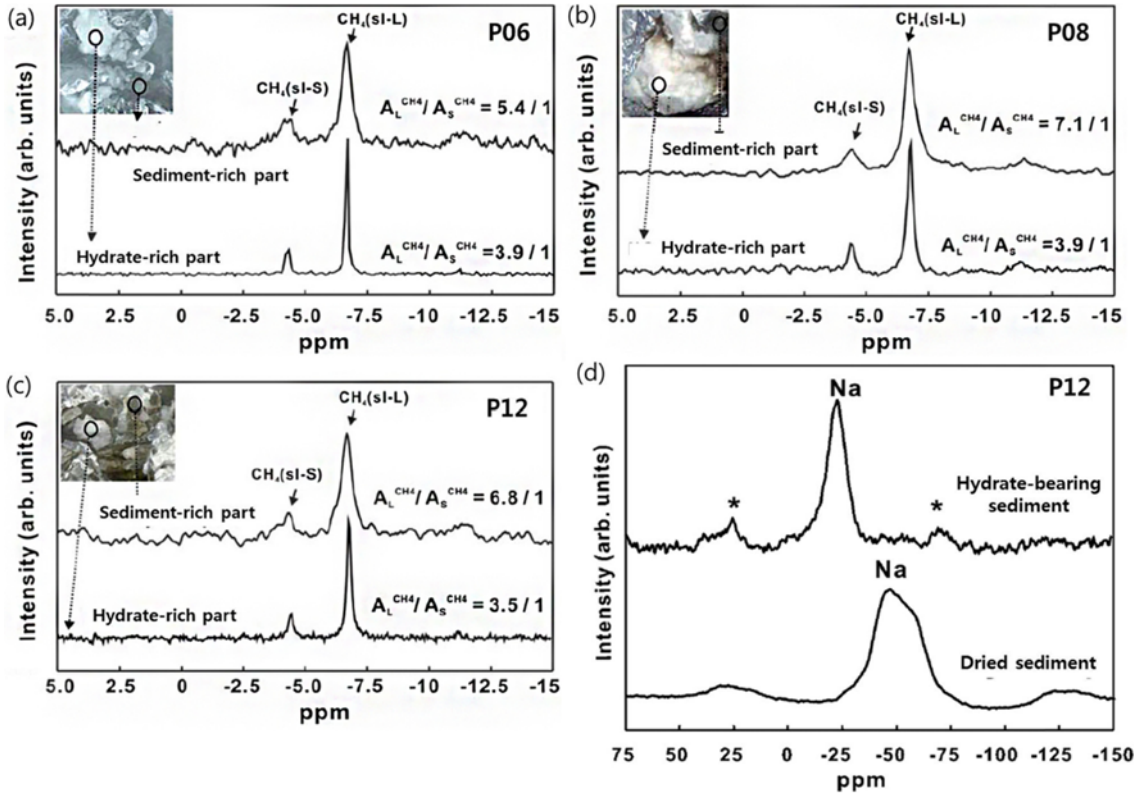

Fig. 10. Solid-state ^{13}C ((a), (b), and (c)) and ^{23}Na (d) NMR of a natural sample recovered from the Ulleung Basin, Piston cores P06, P08, and P12. Reproduced with permission from [92].

et al. [92] proposed that interlayer cations may affect the methane hydrate formation and cage occupancy not only of the artificial methane hydrate, but also of the naturally-occurring hydrate in deep ocean sediment. Even though many other cations exist in the natural ocean sediment, the behaviors of those cations might not substantially differ from those of the sodium cations. Yeon et al. [92] also concluded that the interlayer cation effects on the methane hydrate need to be carefully considered for the gas hydrate recovery. However, further studies should be carried out to collect more information of the complex effect of interlayer cations.

More recently, Ulleung Basin Gas Hydrate Expedition 2 (UBGH2, 2010) provided indisputable evidence for the presence of brine patches at Sites UBGH2-3 and UBGH2-7 [14]. A brine patch represents the massive hydrate deposits co-existing with highly enriched brine pore fluid within shallow depth (upper ~50 m) from the seafloor such as the ODP Leg Site 1249 as discussed in the previous section. Figs. 11(a) and (b) show the chlorinity profiles and volume fraction of gas hydrate of Site UBGH2-3 and Site UBGH2-7. The chlorinity values are up to about 1,500 mM for Site UBGH2-3 and 800 mM for Site UBGH2-7 with extensively saturated gas hydrate in pore space. However, neither an increase in the pore fluid chlorinity nor the accumulation of gas hydrate near the seafloor was detected at Site UBGH2-2-1 (related to only a truncated chimney), as shown in Fig. 11(c).

From the several recent seismic surveys, the Ulleung Basin is characterized by an abundance of columnar acoustic blanking structures (seismic chimneys or gas chimneys) that are up to 2 km wide [13,14,19,45]. These seismic chimneys probably represent vertical conduits for gas originating from below the BGHSZ. They mostly terminate within the RGHSZ, but a few extend to the seafloor to form pockmarks or hydrate mounds (Fig. 12). The results of the site survey collectively suggest that the near seafloor gas hydrates are related to seismic chimneys extended to the seafloor (e.g. Sites UBGH2-3 and UBGH2-7).

The seismic surveys of UBGH2 revealed the existence of matured chimneys obviously extending to the seafloor Sites UBGH2-3 and UBGH2-7. Especially in the recovered core from Site UBGH2-7, the normal faults and fractures which may be migration pathways for methane free gas can be observed by the naked eye to be massive and nodular gas hydrate [14] (Fig. 12). There is no evidence for distinct methane plumes, nor for significant chemosynthetic communities [94]. Methane plumes and chemosynthetic communities characterize the active methane seepage sites, such as at other methane seep sites, Site 1249 and U1328. In this respect, Torres et al. [14] suggested that there is no significant methane discharge to the seafloor at Sites UBGH2-3 and UBGH2-7 and all the upward methane may be entrapped in the near-seafloor gas hydrate deposits. In contrast, only a truncated chimney nearby Site UBGH2-2-1 was detected, through which the gas transport ends within the RGHSZ. Gas hydrate accumulations here are just related to coarse sediment layers [95], and there are no massive hydrates near the seafloor or positive chlorinity development. It is not yet clear whether the chimneys in the Ulleung Basin represent a young or old stage in the evolution of brine patches [14]. Further extensive studies including authigenic carbonate and pore water analyses and detailed seafloor surveys are needed to establish the complicated surroundings and history

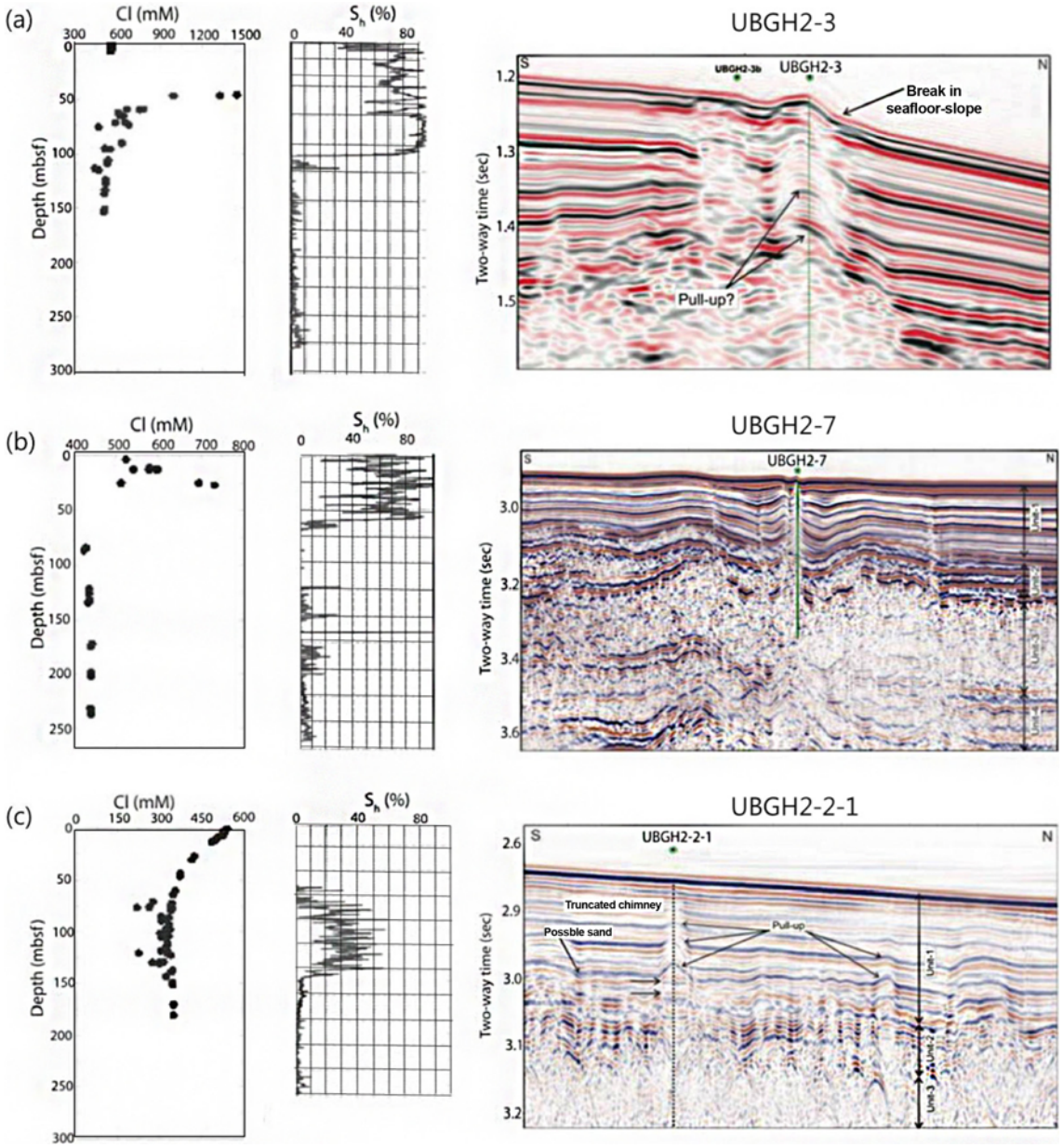

Fig. 11. Chlorinity, volume fraction of hydrate, and seismic data of UBGH2-3 (a), UBGH2-7 (b), and UBGH2-2-1 (c). Reproduced and modified from [14].

of the brine patches in the Ulleung Basin.

As discussed above, several researchers suggested that around 10^2 mol•m^{-2}•yr^{-1} or more would be needed to enrich chloride and maintain elevated chlorinity induced by extensive hydrate formation rates [72,73,78]. Using this as a minimum methane flux feeding into the brine patches, the hydrate deposits near the seafloor of the Ulleung Basin formed in the time range from 1,000 to 3,000 years [14], although more information such as the volume fraction of hydrate should be accurately confined. Torres et al. [73] estimated that brine patches observed at the southern summit of Hydrate Ridge would form in a time range of 500 to 1,500 years using their one-dimensional models of the positive chlorinity. In contrast, the disseminated gas hydrate deposits in the Blake Ridge are at least 40,000 years old based on the time to dissipate the enriched chloride during gas hydrate formation [60]. Torres et al. [14] also proposed that methane carbon ranging from 0.5 to 5 Mt may be accumulated in each of the brine patches in the Ulleung Basin. Based on the number of gas chimneys extending to the seafloor, there are ~30 brine patches, and then near-seafloor gas hydrate deposits may sequester about 120 Mt of carbon in the Ulleung Basin. Because the Ulleung Basin is comparable to other sites elsewhere that host brine patches, Torres et al. [14] assumed that the global brine patches may contain an amount of carbon in the order of 10^2 Gt, which would be about 1-10% of the total amount of carbon trapped in global natural gas hydrate.

CONCLUSIONS

We have discussed the formation and structure patterns of global natural gas hydrate, including the origins of hydrocarbon, crystal structures, and unique structure transition. We have also announced

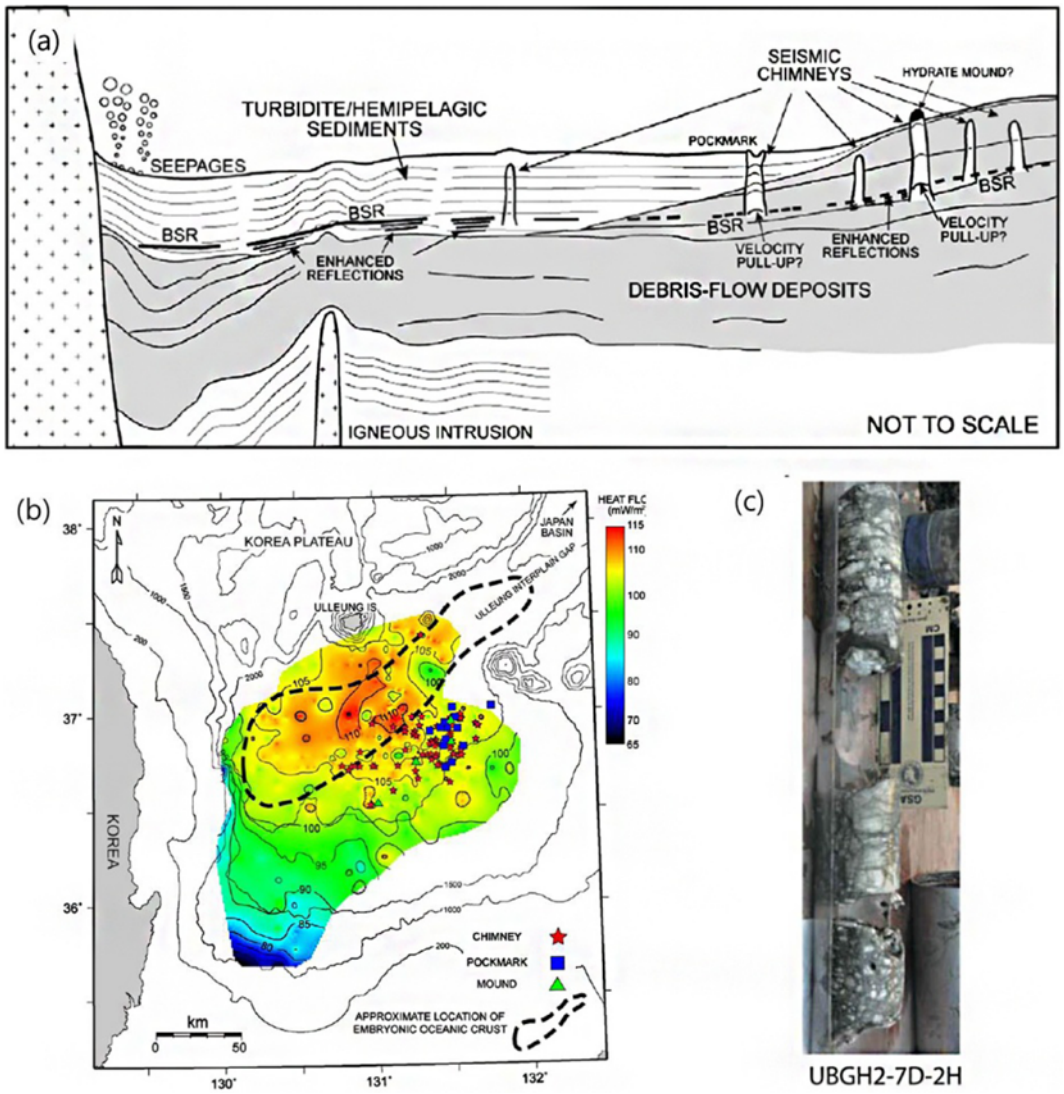

Fig. 12. Schematic (a) and distribution (b) of geological features in the Ulleung Basin; (c), Core sample from UBGH2-7. Reproduced with permission from [(a) and (b), [13]; (c), [14]].

two important anomalies related to methane occupancy and chlorinity, which were revealed very recently. Furthermore, we have reviewed the geological and chemical surroundings of the shallow hydrate deposits, so-called brine patch discovered in the Cascadia Margin and Ulleung Basin, which are significantly related to tectonic conduits for methane gas and positive chlorinity. The near-surface hydrates over the world, which are often related to highly enriched chloride, may contain 1-10% of total amount of carbon in global natural gas hydrate. Although it seems to be a relatively small amount, this type of shallow concentrated hydrate may be more susceptible to fluctuations of pressure, temperature, and salinity. Some researchers do not consider the shallow hydrates as targets for production for technical and safety reasons [96]. The gas production infrastructures installed near the seafloor can transmit various stresses, such as heat, to the shallow hydrates [9]. Of course, this sensitivity of shallow hydrates would act not only as an advantage to gas hydrate production, but also as hazard factor to ocean ecosystems and cause global warming.

Boswell et al. [9] categorized the industrial geohazards related to the gas hydrate production as four types: (1) installation of infrastructure in areas of shallow hydrate, (2) shallow drilling and well-installation targeting deeper horizons, (3) long-term hazards associated with producing warm hydrocarbons from deeper zones through shallow hydrate layer, and (4) geochemical failure of reservoir during production. Generally, because the presence of gas hydrate increases the mechanical strength of the hydrate-bearing sediment, dissociation of that gas hydrate releases free gas and excess pore water and can remarkably reduce the geochemical stability of the sediment layer [9]. Especially, shallow hydrate deposits are little consolidated and the hydrate supports mechanical construction. For example, production by depressurization may be followed by reservoir compaction and overlaying sediments subsidence. It is hoped that geomechanical stability could be maintained with the swapping process, such as CO_2-CH_4 and CO_2/N_2-CH_4 [5-7,97]. Recently, Park et al. [6] suggested that CO_2/N_2 gas mixture (20 mol% of CO_2) is more efficient than pure CO_2 to produce CH_4 from artificial methane hydrate. Koh et al. [98] also experimentally demonstrated that CO_2/N_2 mixture shows higher efficiency (~20%) than pure CO_2 even

for a NGH sample recovered from the East Sea. The methods of oil and gas production from a conventional reservoir can also cause the thermal destabilization of shallow hydrate due to heated wellbores [99,100]. The most important consideration is that sufficient understanding and accurate analyses of the complex surroundings in natural system must occur before we can apply the methane recovery process to real systems to optimize the process and preserve the ocean environment.

ACKNOWLEDGEMENT

This work was supported by the National Research Foundation of Korea government (MEST) (No. 2010-0029176, WCU program: 31-2008-000-10055-0). This research was also supported by the Ministry of Knowledge Economy through the Recovery/Production of Natural Gas Hydrate using Swapping Technique (KIGAM - Gas Hydrate R&D Organization).

REFERENCES

1. K. A. Kvenvolden and T. D. Lorenson, in *Natural gas hydrates; occurrence, distribution, and detection*, C. K. Paull and W. P. Dillon Eds., American Geophysical Union, Washington DC, Geophysical Monograph, **124**, 3-18 (2001).
2. K. A. Kvenvolden, *Proc. Natl. Acad. Sci. USA*, **96**, 3420 (1999).
3. J. Seol, J.-W. Lee, D.-Y. Kim, S. Takeya, J. A. Ripmeester and H. Lee, *J. Phys. Chem. B*, **114**, 804 (2010a).
4. J. Seol, J.-W. Lee, W. Shin, D.-Y. Koh, J. Lee and H. Lee, *J. Phys. Chem. C*, **114**, 17960 (2010b).
5. H. Lee, Y. Seo, Y.-T. Seo, I. L. Moudrakovski and J. A. Ripmeester, *Angew. Chem. Int. Ed.*, **115**, 5202 (2003).
6. Y. Park, D.-Y. Kim, J.-W. Lee, D.-G. Huh, K.-P. Park, J. Lee and H. Lee, *Proc. Natl. Acad. Sci. USA*, **103**, 12690 (2006).
7. K. Shin, Y. Park, M. Cha, K.-P. Park, D.-G. Huh, J. Lee, S.-J. Kim and H. Lee, *Energy & Fuels*, **22**, 3160 (2008).
8. R. Boswell and T. Collett, *FITI*, **6**(3), 5 (2006).
9. R. Boswell, T. Collett, S. Dallimore and M. Frye, *FITI*, **12**(1), 11 (2012).
10. J. C. Santamarina and J. Jang, *FITI*, **9**(4), 18 (2009).
11. A. H. Johnson, *FITI*, **11**(2), 1 (2011).
12. A. M. Tréhu, G. Bohrmann, F. R. Rack and M. E. Torres, *Proceedings of ODP, Initial Reports 204*, [online] http://www-odp.tamu.edu/publications/e04_IR/204ir.htm (2003).
13. S. Horozal, G. H. Lee, B. Y. Yi, D. G. Yoo, K. P. Park, H. Y. Lee, W. Kim, H. J. Kim and K. Lee, *Mar. Geol.*, **258**, 126 (2009).
14. M. E. Torres, J. H. Kim, J.-Y. Choi, B.-J. Ryu, J.-J. Bahk, M. Riedel, T. S. Collett, W.-L. Hong and M. Kastner, *Proceedings of the 7th international conference on gas hydrates*, Edinburgh, Scotland, United Kingdom (2011).
15. R. Sassen, S. T. Sweet, A. V. Milkov, D. A. DeFreitas and M. C. Kennicutt, in *Natural gas hydrates; occurrence, distribution, and detection*, C. K. Paull and W. P. Dillon Eds., American Geophysical Union, Washington DC, Geophysical Monograph, **124**, 131 (2001).
16. J. Ashi, S. Saito, K. Aoike, T. Toki, T. Kuramoto and P. Henry, *EOS Transaction*, American Geophysical Union, **83**, Fall meeting supplement (Abstract), T11B-1248 (2002).
17. E. Suess, M. E. Torres, G. Bohrmann, R. W. Collier, D. Rickert, C. Goldfinger, P. Linke, A. Heuser, H. Sahling, K. Heeschen, C. Jung, K. Nakamura, J. Greinert, O. Pfannkuche, A. M. Tréhu, G. Klinkhamer, M. J. Whiticar, A. Eisenhauer, B. Teichert and M. Elvert, in *Natural gas hydrates; occurrence, distribution, and detection*, C. K. Paull and W. P. Dillon Eds., American Geophysical Union, Washington DC, Geophysical Monograph, **124**, 87 (2001).
18. A. V. Milkov, G. R. Dickens, G. E. Claypool, Y.-J. Lee, W. S. Borowski, M. E. Torres, W. Xu, H. Tomaru, A. M. Tréhu and P. Schultheiss, *Earth Planet. Sci. Lett.*, **222**, 829 (2004).
19. J. J. Bahk, J.-H. Kim, G.-S. Kong, Y. Park, H. Lee, Y. Park and K. P. Park, *Geosci. J.*, **13**, 371 (2009).
20. C. K. Paull, W. Ussler and W. S. Borowski, in *International conference on natural gas hydrates*, E. D. Sloan, J. Happel and M. A. Hnaow Eds., Annals of the New York Academy of Sciences, **715**, 392 (1994).
21. M. J. Whiticar, E. F. Faber and M. Schoell, *Geochim. Cosmochim. Acta*, **50**, 693 (1986).
22. M. J. Whiticar, *Chem. Geol.*, **161**, 291 (1999).
23. M. Schoell, *Chem. Geol.*, **71**, 1 (1988).
24. J. M. Brooks, M. C. Kennicutt, R. R. Fey, T. J. McDonald and R. Sassen, *Science*, **225**, 409 (1984).
25. G. D. Ginsburg, in *Gas hydrates: Relevance to world margin stability and climatic change*, J.-P. Henriet and J. Mienert, Eds., Geological Society, London, Special Publication, **137**, 51 (1998).
26. A. V. Milkov, G. E. Claypool, Y. J. Lee and R. Sassen, *Geochim. Cosmochim. Acta*, **69**, 1007 (2005).
27. N. R. Champman, J. W. Pohlman, R. B. Coffin, J. P. Chanton and L. Lapham, *EOS Trans.*, **85**, 361 (2004).
28. J. W. Pohlman, E. A. Canuel, N. R. Chapman, G. D. Spence, M. J. Whiticar and R. B. Coffin, *Org. Geochem.*, **36**, 703 (2005).
29. R. Matsumoto, H. Tomaru, A. Hiruta, Y. Ishida, R. Takeuchi, G. Snyder, R. Kotani, Y. Okuda, M. Sato, H. Numanami, C. Aoyama, M. Hiromatsu, H. Lu, N. S. Matsuda, Z. Lu, E. Takeuchi, T. Goto, H. Machiyama, H. Toh and J. Komatsubara, *American geophysical union fall meeting*, Abstract no.OS41C-04 (2005).
30. R. Sassen, S. T. Sweet, A. V. Milkov, D. A. DeFreitas and M. C. Kennicutt, *Geology*, **29**, 107 (2001).
31. R. Sassen and I. R. Mcdonald, *Org. Geochem.*, **22**, 1029 (1994).
32. R. Sassen, S. Joye, S. E. Sweet, D. A. DeFreias, A. V. Milkov and I. R. McDonald, *Org. Geochem.*, **30**, 485 (1999).
33. J. M. Brooks, B. H. Cox, W. R. Bryant, M. C. Kennicutt, R. G. Mann and T. J. McDonald, *Org. Geochem.*, **10**, 221 (1986).
34. J. M. Brooks, M. E. Field and M. C. Kennicutt, *Marine Geol.*, **96**, 103 (1991).
35. G. Ginsburg, A. N. Kremlev, M. N. Grigor'ev, G. V. Larkin, A. D. Pavlenkin and N. A. Saltykova, *Geologiyai Geofizika*, **313**, 10 (1990).
36. V. N. Blinova, M. K. Ivanov and G. Bohrmann, *Geo-Mar. Lett.*, **23**, 250 (2003).
37. G. D. Ginsburg, R. A. Guseynov, A. A. Dadashev, G. A. Ivanova, S. A. Kazantsev, V. A. Soloviev, E. V. Telepnev, P. Ye. Askefi-Nasinov, A. A. Yesikov, V. I. Mal'tseva, G. Yu. Mashirov and I. Yu. Shabayeva, *Int. Geol. Rev.*, **43**, 765 (1992).
38. G. Ginsburg, V. A. Soloviev, R. E. Cranston, T. D. Lorenson and K. A. Kvenvolden, *Geo-Mar. Lett.*, **13**, 41 (1993).
39. K. A. Kvenvolden and M. Kastner, in *Proceedings of ocean drilling program, scientific results*, **112**, E. Suess and R. von Huene, et

al. Eds., College station, TX, 517-526 (1990).
40. T. S. Collett, *Am. Assoc. Petrol. Geol. Bull.*, **77**, 793 (1993).
41. T. D. Lorenson, M. J. Whiticar, A. Waseda, S. R. Dallimore and T. S. Collett, in *Scientific Results from JAPEX.JNOC/GSC Mallik 2L-38 Gas Hydrate Research Well, Mackenzie Delta, Northwest Territories, Canada*, S. R. Dallimore, T. Uchida and T. S. Collett Eds., Geological Survey of Canada Bulletin, **544**, 143 (1999).
42. T. D. Lorenson and T. S. Collett, in *Proceedings of ocean drilling program*, C. K. Paull, R. Matsumoto, P. J. Wallace and W. P. Dillon Eds., College Station, TX, 37-46 (2000).
43. A. Waseda and T. Uchida, *Proceedings of 4th International Conference on Gas Hydrates, Yokohama, Japan*, 19-174 (2002).
44. J. H. Kim, M.-H. Park and J.-H. Chun, *Geo-Mar. Lett.*, **31**, 37 (2011).
45. J. H. Kim, M. E. Torres, J. Choi, J.-J. Bahk, M.-H. Park and W. L. Hong, *Org. Geochem.*, **43**, 26 (2012).
46. D. W. Davidson, S. K. Garg, S. R. Gough, Y. P. Handa, C. I. Ratcliffe, J. A. Ripmeester, J. S. Tse and W. F. Lawson, *Geochim. Cosmochim. Acta*, **50**, 619 (1986).
47. J. A. Ripmeester, J. S. Tse, C. I. Ratcliffe and B. N. Powell, *Nature*, **325**, 135 (1987).
48. H. Lu, Y. Seo, J. Lee, I. Moudrakovski, J. A. Ripmeester, N. R. Chapman, R. B. Coffin, G. Gardner and J. Pohlman, *Nature*, **445**, 303 (2007).
49. S.-H. Yeon, J. Seol and H. Lee, *J. Am. Chem. Soc.*, **128**, 12388 (2006).
50. R. E. Grim, Clay Mineralogy, 2nd Ed., McGraw-Hill (1968).
51. H. Ouar, S. B. Cha, T. R. Wildeman and E. D. Sloan, *Chem. Eng. Res. Des.*, **70**, 48 (1992).
52. R. E. Grim and G. Kulbicki, *Am. Mineral.*, **46**, 1329 (1961).
53. S. B. Cha, H. Ouar, T. R. Wildeman and E. D. Sloan, *J. Phys. Chem.*, **92**, 6492 (1988).
54. S.-H. Yeon, J. Seol, Y. Seo, Y. Park, D.-Y. Koh, K.-P. Park, D.-G. Huh, J. Lee and H. Lee, *J. Phys. Chem. B Lett.*, **113,** 245 (2009).
55. Y. Seo, J. Seol, S.-H. Yeon, D.-Y. Koh, M. Cha, S.-P. Kang, Y.-T. Seo, J. Bahk, J. Lee and H. Lee, *J. Chem. Eng. Data*, **54**, 1284 (2009).
56. E. M. Chuvilin, E. V. Kozlova, N. A. Makhonina, V. S. Yakushew and D. V. Dubinyak, *Proceedings of 4th International Conference on Gas Hydrates*, 433-438 (2002).
57. S. Guggenheim and A. F. Koster van Groos, *Geology*, **31**, 653 (2003).
58. P. Englezos and S. Hall, *Can. J. Chem. Eng.*, **72**, 887 (1994).
59. K. M. Lee, H. Lee, J.-H. Lee and J. M. Kang, *Geophy. Res. Lett.*, **29**, 2034 (2002).
60. W. Ussler and C. K. Paull, in *Natural gas hydrates; occurrence, distribution, and detection*, C. K. Paull and W. P. Dillon Eds., American Geophysical Union, Washington DC, Geophysical Monograph, **124**, 41 (2001).
61. W. E. Harrison, R. Hesse and J. M. Gieskes, in *Initial reports of the deep sea drilling project*, J. Aubouin, et al., Eds., U. S. Government Printing Office, Washington, D.C. (1982).
62. J. M. Gieskes, K. Johnston and M. Boehm, in *Initial reports of the deep sea drilling project*, R. von Huene, et al. Eds., U.S. Government Printing Office, Washington, D.C. (1985).
63. K. A. Kvenvolden and L. A. Barnard, *Initial Reports, Deep Sea Drilling Project*, **76**, 353 (1983).
64. P. D. Jenden and J. M. Gieskes, *Initial Reports Deep Sea Drilling Project*, **76**, 453 (1983).
65. C. K. Paull, T. D. Lorenson, W. S. Boroworski, W. Ussler, K. Olsen, N. M. Rodriguez and H. Wehner, *Proceedings of Ocean Drilling Program Scientific Results*, **164**, 67 (2000).
66. K. A. Kvenvolden and T. J. Mcdonald, *Initial Reports, Deep Sea Drilling Project*, **84**, 667 (1985).
67. R. Hesse, J. Lebel and J. M. Gieskes, *Initial Reports, Deep Sea Drilling Project*, **84**, 727 (1985).
68. M. J. Whiticar, M. Hovland, M. Kastner and J. C. Sample, *Proc. Ocean Drill. Program, Sci. Results*, **146**, 385 (1995).
69. R. E. Cranston, in *Scientific Results from JAPEX.JNOC/GSC Mallik 2L-38 Gas Hydrate Research Well, Mackenzie Delta, Northwest Territories, Canada*, S. R. Dallimore, T. Uchida and T. S. Collett Eds., Geological Survey of Canada Bulletin, **544**, 295 (1999).
70. P. K. Egeberg and G. R. Dickens, *Chem. Geol.*, **153**, 53 (1999).
71. M. K. Davie and B. A. Buffet, *J. Geophys. Res.*, **106**, 497 (2001).
72. M. Haeckel, E. Suess, K. Wallman and E. Rickert, *Geochim. Cosmochim. Acta*, **68**, 4335 (2004).
73. M. E. Torres, K. Wallmann, A. M. Tréhu, G. Bohrmann, W. S. Borowski and H. Tomaru, *Earth Planet. Sci. Lett.*, **226**, 225 (2004).
74. B. A. Buffett and O. Y. Zatsepina, *Marine Geol.*, **164**, 69 (1999).
75. X. Liu and P. B. Flemings, *Earth Planet. Sci. Lett.*, **241**, 211 (2006).
76. H. Daigle and B. Dugan, *Geophys. Res. Lett.*, **37**, L20301 (2010).
77. R. Hesse, *Earth Sci. Rev.*, **61**, 149 (2003).
78. J. Seol, D.-Y. Koh, M. Cha, W. Shin, Y.-J. Lee, J.-H. Kim, J. Lee and H. Lee, *AIChE J.* **58**, 322 (2012).
79. E. Suess, M. E. Torres, G. Bohrmann, R. W. Collier, J. Greinert, P. Linke, G. Rehder, A. M. Tréhu, K. Wallmann, G. Winckler and E. Zuleger, *Earth Planet. Sci. Lett.*, **170**, 1 (1999).
80. A. M. Tréhu, N. L. Bangs, M. A. Arsenault, G. Bohrmann, C. Goldfinger, J. E. Johnson, Y. Nakamura and M. E. Torres, *Proceedings of the 4th International Gas Hydrate, Yokohama, Japan*, 90-96 (2002).
81. D.-Y. Kim, T.-W. Uhm, H. Lee, Y.-J. Lee, B.-J. Ryu and J.-H. Kim, *Korean J. Chem. Eng.*, **22**, 569 (2005).
82. K. C. Hester, R. M. Dunk, S. N. White, P. G. Brewer, E. T. Peltzer and E. D. Sloan, *Geochim. Cosmochim. Acta*, **71**, 2947 (2007).
83. A. M. Tréhu, P. E. Long, M. E. Torres, G. Bohrmann, F. R. Rack, T. S. Collett, D. S. Goldberg, A. V. Milkov, M. Ridel, P. Schultheiss, N. L. Bangs, S. R. Barr, W. S. Borowski, G. E. Claypool, M. E. Delwiche, G. R. Dickens, E. Gracia, G. Guerin, M. Holland, J. E. Johnson, Y.-J. Lee, C.-S. Liu, X. Su, B. Teichert, H. Tomaru, M. Vanneste, M. Watanabe and J. L. Weinberger, *Earth Planet. Sci. Lett.*, **222**, 845 (2004).
84. K. U. Heeschen, R. W. Collier, M. A. de Angelis, E. Suess, G. Rehder, P. Linke and G. P. Klinkhammer, *Glob. Biogeochem. Cycles*, **19**, GB2016 (2005).
85. A. V. Milkov and W. Xu, *Earth Planet. Sci. Lett.*, **239**, 162 (2005).
86. M. E. Torres, J. McManus, D. E. Hammond, M. A. de Angelis, K. U. Heeschen, S. L. Colbert, M. D. Tryon, K. M. Brown and E. Suess, *Earth Planet. Sci. Lett.*, **201**, 525 (2002).
87. M. Hovland, *Cont. Shelf Res.*, **22**, 2387 (2002).
88. K. U. Heeschen, A. M. Tréhu, R. W. Collier, E. Suess and G. Rehder, *Geophys. Res. Lett.*, **30**, 1643 (2003).
89. J. H. Lee, Y. S. Baek, B. J. Ryu, M. Riedel and R. D. Hyndman, *Mar. Geophy. Res.*, **26**, 51 (2005).
90. J.-J. Bahk, I.-K. Um and M. Holland, *Mar. Petrol. Geol.*, **28**, 1943 (2011).
91. B.-J. Ryu, M. Riedel, J.-H. Kim, R. D. Hyndman, Y.-J. Lee, B.-H. Chung and I.-S. Kim, *Mar. Petrol. Geol.*, **26**, 1483 (2009).

92. S.-H. Yeon, J. Seol, D.-Y. Koh, Y. Seo, K.-P. Park, D.-G. Huh, J. Lee and H. Lee, *Energy. Environ. Sci.*, **4**, 421 (2011).
93. K.-P. Park, J.-J. Bahk, Y. Kwon, G. Y. Kim, M. Riedel, M. Holland, P. Schultheiss, K. Rose and the UBGH-1 scientific party, *FITI*, **8**(2), 6 (2008).
94. KIGAM, *Studies on Gas Hydrate Geology, Geochemistry and Stability, NP2008-003-2009*, Gwacheon, Republic of Korea: Ministry of Knowledge Economy (2009).
95. UBGH2 scientists, *Preliminary Report*, Daejeon, Republic of Korea, KIGAM (2010).
96. C. Ruppel, T. Collet, R. Boswell, T. Lorenson, B. Buczkowski and W. Waite, *FITI*, **11**(1), 13 (2011).
97. H. Farrell, R. Boswell, J. Howard and R. Baker, *FITI*, **10**(1), 19 (2010).
98. D.-Y. Koh, H. Kang, D.-O. Kim, J. Park, M. Cha and H. Lee, *ChemSusChem*., **5**, 1443 (2012).
99. D. Peters, G. Hatton, A. Mehta and C. Hadley, *Proceedings of the 6th International Conference on Gas Hydrates* (2008).
100. J. Rutqvist and G. J. Moridis, *SPE J.*, **14**, 267 (2009).

Huen Lee is currently a KEPCO Chair Professor in the Department of Chemical and Biomolecular Engineering, KAIST. He obtained his Ph.D. in Chemical Engineering Thermodynamics from Northwestern University, USA in 1983. He worked for two years at KIST before joining KAIST in 1985. He was a visiting professor at the University of California, Berkeley. He is now in charge of Energy and Environmental System Laboratory, focusing on hydrogen storage, carbon sequestration and gas hydrate.